
The Less You Depend, The More You Learn: Synthesizing Novel Views from Sparse, Unposed Images without Any 3D Knowledge

Haoru Wang^{1,*}, Kai Ye^{1,*}, Yangyan Li^{2,†}, Wenzheng Chen^{1,†}, Baoquan Chen^{1,†}

¹Peking University ²AMAP

ou524u@stu.pku.edu.cn, ye_kai@pku.edu.cn, yangyan.lyy@alibaba-inc.com,
wenzhengchen@pku.edu.cn, baoquan@pku.edu.cn

Abstract

We consider the problem of generalizable novel view synthesis (NVS), which aims to generate photorealistic novel views from sparse or even unposed 2D images without per-scene optimization. This task remains fundamentally challenging, as it requires inferring 3D structure from incomplete and ambiguous 2D observations. Early approaches typically rely on strong 3D knowledge, including architectural 3D inductive biases (*e.g.*, embedding explicit 3D representations, such as NeRF or 3DGS, into network design) and ground-truth camera poses for both input and target views. While recent efforts have sought to reduce the 3D inductive bias or the dependence on known camera poses of input views, critical questions regarding the role of 3D knowledge and the necessity of circumventing its use remain under-explored. In this work, we conduct a systematic analysis on the 3D knowledge and uncover a critical trend: the performance of methods that requires less 3D knowledge accelerates more as data scales, eventually achieving performance on par with their 3D knowledge-driven counterparts, which highlights the increasing importance of reducing dependence on 3D knowledge in the era of large-scale data. Motivated by and following this trend, we propose a novel NVS framework that minimizes 3D inductive bias and pose dependence for both input and target views. By eliminating these 3D knowledge, our method fully leverages data scaling and learns implicit 3D awareness directly from sparse 2D images—without any 3D inductive bias or pose annotation during training. Extensive experiments demonstrate that our model generates photorealistic and 3D-consistent novel views, achieving even comparable performance with methods that rely on posed inputs, thereby validating the feasibility and effectiveness of our data-centric paradigm. Project page: <https://pku-vc1-geometry.github.io/Less3Depend/>.

1 Introduction

Reconstructing 3D scenes and synthesizing novel views from 2D observations has been a long-standing goal in computer vision and graphics. One of the most challenging settings in this domain is generalizable novel view synthesis (NVS), which aims to generate photorealistic views of a scene from a few sparse, wide-baseline, or even unposed input images. While humans can effortlessly understand coherent 3D structure from sparse and ambiguous 2D cues, this task remains difficult for machines, as it requires recovering accurate 3D structure from sparse, incomplete 2D observations, particularly without camera pose information for both input and target views.

To address this challenge, previous works mainly exploit large-scale training data across diverse scenes to enable NVS generalization for new inputs at inference time. These methods [50, 36, 12, 5, 6, 48, 18]

*Equal contribution. †Equal advisory.

typically design networks that take sparse views as input, learning to infer the underlying 3D scene structure and synthesize its novel views. More importantly, their design of networks depend heavily on **3D knowledge**, which appears at multiple levels of the learning pipeline. For instance, such 3D knowledge may be encoded as **3D inductive bias** (i.e., explicit 3D representations embedded in the network architecture), in the **input data** (e.g., ground-truth camera poses for input views), or in the **training supervision** (e.g., optimizing target views using known poses). Such dependence on 3D knowledge further shapes the problem settings of the generalizable NVS task. As illustrated in Figure 1, we categorize the task into three settings based on the pose availability: the *posed* setting, where both input and target poses are provided; the *posed-target* setting, where only the target pose is available; and the *unposed* setting, where only images are provided, without any pose information.

Early methods such as PixelNeRF [50], PixelSplat [5], and MVsplat [6] mainly address posed setting and incorporate strong 3D knowledge. For example, they typically embed 3D inductive bias into the architecture, modeling scenes with neural radiance fields (NeRF [26]) or 3D Gaussian Splatting (3DGS [20]), and relying on ground-truth poses for both input and target views during training. In contrast, recent methods such as DUST3R [43], LVSM [18], NoPoSplat [48], and VGGT [41] reduce such dependence on 3D knowledge and start to explore more challenging posed-target setting. For instance, they remove inductive bias in network design and learn implicit spatial reasoning. Several methods [48, 43, 41] further eliminate pose requirements for input views. Trained on large-scale posed image collections, these approaches have demonstrated promising performance in novel view synthesis. Reconsidering the design of these methods raises two important open questions:

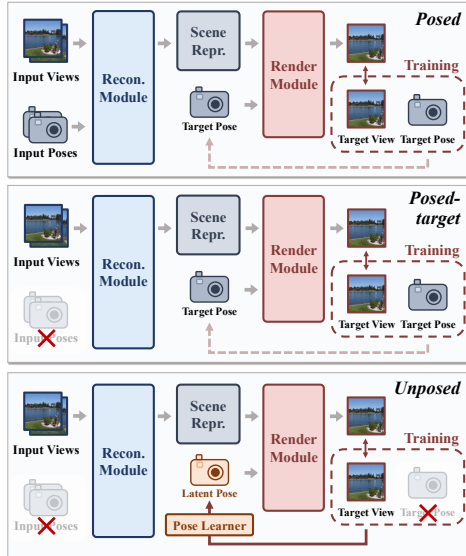


Figure 1: Problem Setting Overview.

- As datasets continue to grow in scale and diversity, which design paradigm offers better scalability? Should future generalizable NVS methodology design incorporate more 3D knowledge, or move in the opposite direction?
- Can neural networks learn NVS under unposed setting, *i.e.*, inferring 3D structure and synthesizing novel views purely from 2D visual observations, without relying on any 3D knowledge—neither 3D inductive bias, nor camera poses in the input or supervision?

In this work, we conduct a comprehensive investigation to address the two questions raised above. We begin by systematically analyzing state-of-the-art methods [6, 48, 18] across varying data regimes and different levels of 3D knowledge under different problem settings. Our experiments reveal a consistent trend: methods with reduced dependence on 3D knowledge demonstrate superior scalability in data-rich environment. In other words, their performance *increases higher* as the amount of training data increases. This exposes a fundamental trade-off: methods with more 3D knowledge, particularly the 3D inductive bias, perform robustly in low-data regimes but become increasingly restrictive as data scales. In contrast, methods with less 3D knowledge benefit more from larger training data and eventually achieve performance on par with—or even surpassing—those with strong 3D knowledge.

Motivated by these findings, we propose a novel generalizable NVS method designed for the most challenging *unposed* setting that eliminates the need for 3D knowledge. Strikingly, our method demonstrates that effective 3D awareness can emerge directly from unposed, sparse-view 2D images—without relying on architectural 3D inductive bias or any pose annotations. While this may seem implausible, we show that it is achievable through a multi-view self-supervised formulation. Specifically, we propose a novel *Latent Plücker Learner* that models spatial relationship between views with latent representations, allowing model to automatically construct the pose space of input and target views. This facilitates learning implicit 3D awareness without any explicit 3D supervision.

Extensive experiments show that our method produces photorealistic and 3D consistent NVS results, achieving competitive performance compared to state-of-the-art approaches that rely on 3D inductive bias or pose annotations. This not only validates the feasibility of minimizing 3D knowledge, but also opens a new path toward scalable, generalizable spatial reasoning purely from 2D observations.

2 Revisiting 3D Knowledge in Generalizable Novel View Synthesis

Novel View Synthesis The novel view synthesis (NVS) problem aims to reconstruct a 3D scene \mathcal{S} from a set of 2D image observations $(\mathcal{I}^i, \mathcal{P}_{\mathcal{I}}^i)_{i=1}^N$, where \mathcal{I}^i is the i -th input image and $\mathcal{P}_{\mathcal{I}}^i$ is its corresponding camera pose. The goal is to render a target image \mathcal{T} from a novel viewpoint $\mathcal{P}_{\mathcal{T}}$ and it is typically supervised by the reconstruction loss L w.r.t. the ground-truth image $\tilde{\mathcal{T}}$:

$$\mathcal{S} = \mathcal{A}(\mathcal{I}^1, \mathcal{P}_{\mathcal{I}}^1, \mathcal{I}^2, \mathcal{P}_{\mathcal{I}}^2, \dots, \mathcal{I}^N, \mathcal{P}_{\mathcal{I}}^N), \quad \mathcal{T} = \mathcal{R}(\mathcal{S}, \mathcal{P}_{\mathcal{T}}), \quad L = \mathcal{L}(\mathcal{T}, \tilde{\mathcal{T}}), \quad (1)$$

where \mathcal{A} is the scene reconstruction function, \mathcal{R} is the rendering function, and \mathcal{L} is the loss function. Once training is done, \mathcal{S} is able to synthesize photorealistic images from novel viewpoints. When the total number of observations is dense ($N \geq 50$), \mathcal{S} is typically optimized as 3D representations such as neural radiance fields (NeRFs [26]) and 3D Gaussian Splatting (3DGS [20]), while \mathcal{R} is the corresponding volumetric or Gaussian Splatting-based rendering formulations.

Generalizable NVS Despite the promise of per-scene optimization approaches, their reliance on dense observations limits their applicability when only sparse or unposed observations are available—typically with $N \leq 5$, and where camera poses $\mathcal{P}_{\mathcal{I}}$ for the input images \mathcal{I} may not be provided. Alternatively, generalizable novel view synthesis [50, 5, 6, 48, 18] seeks to address this challenge by incorporating learning pipelines that leverage learning prior to compensate for the under-constrained setting, like training neural networks to infer the underlying 3D structure from sparse views and synthesize photorealistic novel images. The design of these methods typically involves strong 3D knowledge, including structural inductive bias in network architecture, pose-aware input data, and supervision of target views with known camera poses.

The evolution of generalizable NVS methods can be characterized by their varying reliance on 3D knowledge, which typically manifests in two key aspects: (1) 3D inductive bias in their network design, *i.e.* modeling \mathcal{S} and \mathcal{R} using explicit 3D representations or learn the implicit scenes as latent tokens, and (2) pose availability (*i.e.*, whether input or target view poses are provided), which shape the problem settings.

Method Category We categorize the generalizable NVS problem into three settings: *posed*, *posed-target*, and *unposed*. The posed setting is to reconstruct the scene with known poses for both input and target view, *i.e.*, $\{(\mathcal{I}, \mathcal{P}_{\mathcal{I}}), (\mathcal{T}, \mathcal{P}_{\mathcal{T}})\}$ are both given. The posed-target setting is to reconstruct the scene without input poses but target views are still supervised with poses, *i.e.*, $\{(\mathcal{I},), (\mathcal{T}, \mathcal{P}_{\mathcal{T}})\}$ are provided. Lastly, the unposed setting means no poses are provided, neither for input views nor for target views, *i.e.*, only $\{(\mathcal{I},), (\mathcal{T},)\}$ are provided. Table 1 systematically reviews existing generalizable NVS methods, focusing on their reliance on 3D inductive bias and the problem settings.

Method	w. Inductive Bias	\mathcal{S} Modeling	\mathcal{R} Modeling	Problem Setting	w. $\mathcal{P}_{\mathcal{I}}$	w. $\mathcal{P}_{\mathcal{T}}$
PixelNeRF [50]	✓	NeRF [26]	Volumetric Rendering	posed	✓	✓
PixelSplat [5]	✓	3DGS [20]	Gaussian Splatting		✓	✓
MVSplat [6]	✓	3DGS [20]	Gaussian Splatting		✓	✓
SRT [32]	✗	Latent	Learnable Network		✓	✓
LVSM [18]	✗	Latent	Learnable Network		✓	✓
NoPoSplat [48]	✓	3DGS [20]	Gaussian Splatting	posed-target	✗	✓
Ours (PT-LVSM)	✗	Latent	Learnable Network		✗	✓
RUST [33]	✗	Latent	Learnable Network	unposed	✗	✗
Ours (UP-LVSM)	✗	Latent	Learnable Network		✗	✗

Table 1: **3D Knowledge in Generalizable NVS.** We characterize the evolution of generalizable NVS methods based on their varying dependence on inductive bias (*i.e.*, the choice of \mathcal{S} and \mathcal{R} modeling) and pose availability (whether $\mathcal{P}_{\mathcal{I}}$ and $\mathcal{P}_{\mathcal{T}}$ are provided).

2.1 3D Inductive Bias

Bias-Driven Methods Following LVSM [18], we define 3D inductive bias as explicit 3D representations and handcrafted network designs like epipolar projections or plane sweeps. Methods such as PixelNeRF [50], PixelSplat [5], and MVSplat [6] incorporate NeRF [26] or 3DGS [20] representations along with their corresponding rendering functions, which are particularly effective at capturing cross-view appearance consistency. However, they typically require known camera poses for both input and target views. In the case of NoPoSplat [48], the input poses $\mathcal{P}_{\mathcal{I}}$ are eliminated by leveraging a feed-forward network to initialize 3DGS positions from unposed input images, while still relying on target-view camera poses.

Data-Centric Methods A complementary line of work seeks to model the scene and render novel views in an entirely implicit way, *i.e.*, treating \mathcal{S} as latent tokens without explicitly defined 3D geometry. We refer to these as **data-centric** methods, in contrast to those that incorporate strong 3D inductive bias. Early works such as SRT [32] and RUST [33] adopt a transformer-based architecture to encode the input images \mathcal{I} into tokens. Given a query view $\mathcal{P}_{\mathcal{T}}$, a learnable decoder network acts as the rendering function \mathcal{R} to synthesize the target view \mathcal{T} . While these models demonstrate emerging 3D awareness, they often fall short in generating high-fidelity results due to limited model capacity or insufficient data scale.

Recent advancements, such as LVSM [18], improve rendering quality by combining Plücker ray embeddings and large-scale datasets like RealEstate10K [55]. However, LVSM only addresses the posed setting, requiring known camera poses for both input and target views. In this work, we extend the data-centric design to more challenging scenarios by developing PT-LVSM (Posed-Target Large View Synthesis Model) and UP-LVSM (Unposed Large View Synthesis Model), which generalize the LVSM framework to posed-target and unposed settings, respectively.

2.2 Problem Settings

As mentioned earlier, we categorize the problem settings of the generalized NVS task into three levels based on the availability of camera pose for input views \mathcal{I} and target views \mathcal{T} , as summarized in Table 1. Several interesting facts can be observed. First, all 3D inductive bias-based methods depend on pose annotations—at least for target views during supervision—making them inapplicable to the most challenging unposed setting. In contrast, data-centric methods eliminate the need for 3D inductive bias and offer broader applicability. These approaches can operate under all generalized NVS problem settings, including the posed, posed-target, and unposed scenarios.

2.3 Discussion

While both paradigms—inductive bias-based and data-centric approaches—have shown promising performance, a fundamental question remains underexplored: which paradigm holds greater potential for the future, especially as datasets continue to grow in size and diversity? Our work argues that reducing reliance on 3D knowledge in data-rich environments leads to better scalability, supporting a shift toward minimally constrained, data-driven NVS frameworks that avoid extensive 3D knowledge requirements. We refer to this hypothesis as the principle of *"The less you depend, the more you learn."* Below, we provide a detailed analysis to substantiate this hypothesis.

3 The Less You Depend, The More You Learn

In this section, we present our analysis to validate the hypothesis that *the less you depend, the more you learn*. Specifically, *the less you depend* refers to reducing reliance on 3D knowledge in methodology design, including 3D inductive bias and camera poses for input views. Meanwhile, *the more you learn* refers to scalability, which is defined as how performance improves as the amount of training data increases. By examining the relationship between performance and data quantity for different methods, we find the performance of methods that requires less 3D knowledge accelerates more as data scales.

We first choose the RealEstate10K benchmark [55] for our comparisons, which is one of the largest open-source datasets for generalizable novel view synthesis, containing multi-view imagery from over 70K scenes. We construct subsets of the RealEstate10K dataset at four different scales (little, medium, large, and full, as shown in Table 2) to assess method scalability by examining how performance varies across these different data scales. Note that a consistent test set is used for performance evaluation across all experiments.

An overview comparison results are shown in Figure 2 to highlight the different scalability for state-

Subset	Train	Test
Little	1202	
Medium	4121	7286
Large	16449	
Full	66033	

Table 2: Number of scenes in RealEstate10K [55] subsets.

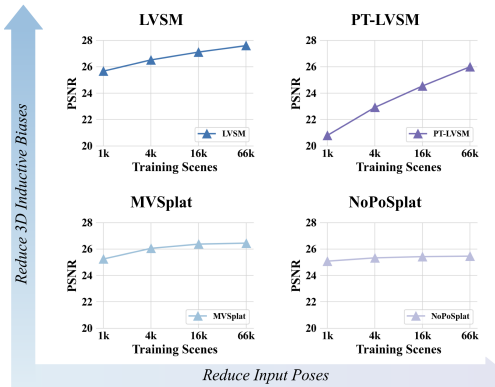


Figure 2: Scalability Overview.

of-the-art methods. We select representative methods that span different levels of reliance on 3D inductive biases and vary in problem settings for our comparisons. For posed setting, we choose MVSpLat [6] as a bias-driven method and LVSM [18] as a bias-free method. For posed-target setting, we select NoPoSplat [48] as the bias-driven method. Given the lack of bias-free solutions for posed-target setting, we extend LVSM [18] to this domain and develop an effective method, PT-LVSM (Posed-Target Large View Synthesis Model), with its detailed implementation provided in Appendix C for clarity. We include PT-LVSM as a representative bias-free solution in posed-target setting comparison to further enhance the comprehensiveness of our analysis.

3.1 Necessity of Minimizing 3D Inductive Bias

An apparent trend can be observed in Figure 2: methods with strong 3D inductive biases (*i.e.*, MVSpLat and NoPoSplat) perform robustly in low-data regimes (*e.g.*, 1K training scenes) but become increasingly restrictive as the data scale increases, demonstrating poor scalability to training data, as shown in Figure 3. In contrast, the data-centric methods (*i.e.*, LVSM and PT-LVSM), although not performing well with only 1K scenes, show significant improvements in performance as the data scales up to 66K, highlighting strong scalability. This not only validates our hypothesis, but also justifies the necessity of minimizing 3D inductive biases in generalizable novel view synthesis, especially given that the available training data will rapidly increase in the future.

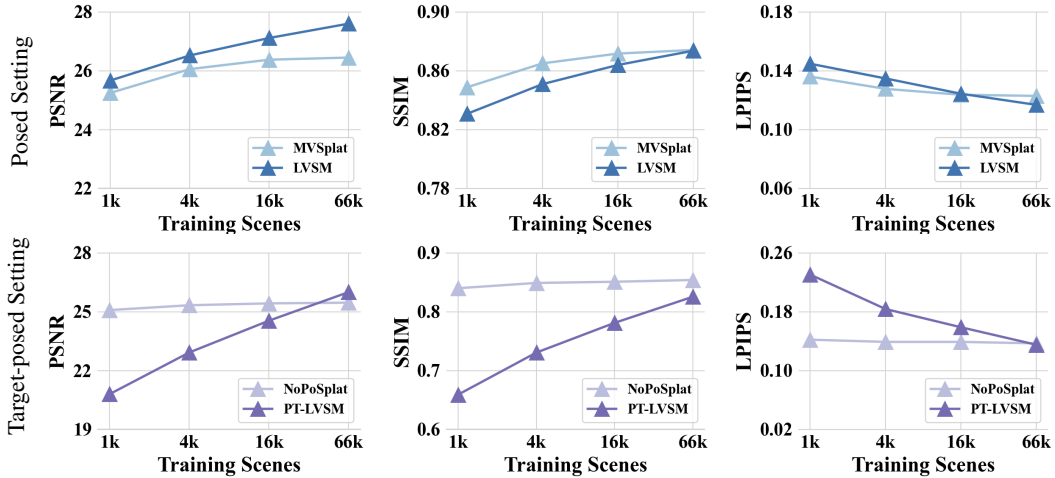


Figure 3: Scalability Comparison on Different Levels of 3D Inductive Bias.

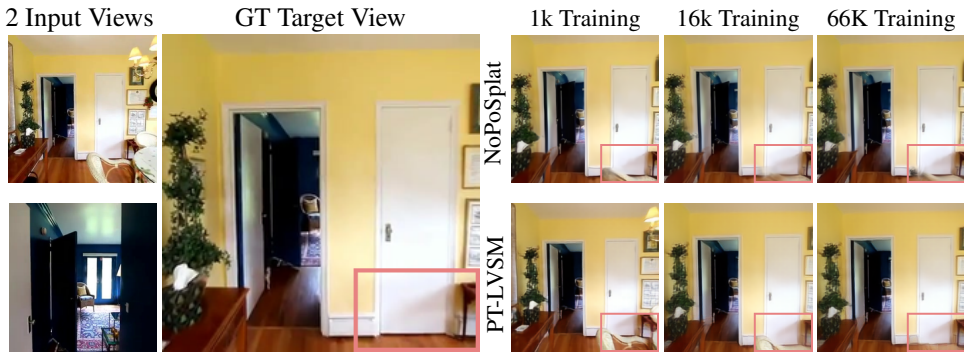


Figure 4: **Intuitive Explanation.** On posed-target setting, both NoPoSplat and PT-LVSM fail to infer correct spatial structure when trained with 1K scenes, resulting in artifacts at the right bottom of target views. While bias-driven NoPoSplat consistently makes mistakes, PT-LVSM significantly improves when training data scales up from 1K to 66K, eventually outperforming NoPoSplat.

Intuitively, when data is scarce, methods face challenges in learning underlying common principles. In such cases, the introduction of human inductive biases can help compensate for the lack of data. However, as the data becomes more abundant, the compensatory benefits of these biases diminish, and the weaknesses—such as biased learning—begin to limit generalization. Figure 4 provides qualitative

results to further illustrate this trend, where the data-centric method improves as the training data increases, while the bias-driven method shows little gains.

3.2 Feasibility of Reducing Pose Annotation

While the impact of 3D inductive bias has been discussed above, we additionally observe a significant increase in scalability from LVSM to PT-LVSM in Figure 2 & 3, which is also illustrated in Figure 5. Although both LVSM and PT-LVSM are data-centric methods with minimal 3D inductive bias, they differ in their problem settings, particularly regarding whether input views are annotated with camera poses.

Intuitively, posed settings provide more information, so for the same input views, a method that can utilize pose information (i.e., posed-setting method) is expected to achieve a higher performance upper bound compared to an unposed-setting method. However, our comparisons suggest that this gap can be mitigated by rich training data. We find that PT-LVSM generally exhibits stronger scalability than LVSM, and based on the scalability trend, PT-LVSM is expected to achieve comparable performance to LVSM when the training data scales up by about 4 times to 64 times. This further suggests that completely reducing the pose annotation for both inference time and training time could be a feasible direction. We hypothesize that the scalability advantage of pose-free learning stems from the noise in supervision, as pose annotations in real-world datasets [55, 47, 49, 23] are typically generated by Structure-from-Motion (SfM) tools [34, 2], which can be error-prone and sensitive to scene conditions.

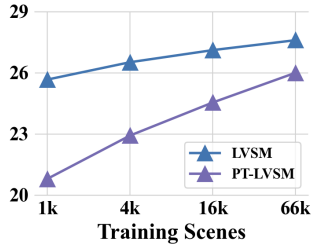


Figure 5: Scalability of LVSM and PT-LVSM.

Motivated by this, we believe that a data-centric framework with minimal 3D knowledge dependence holds great potential in learning spatial reasoning directly from sparse, unposed 2D images. To this end, we propose a novel generalizable NVS framework that reduces dependence on any 3D inductive bias or camera pose. By eliminating these 3D knowledge, our method fully capitalizes on data scalability at large scales, delivering competitive performance compared to state-of-the-art approaches, even with purely 2D supervision. We will provide detailed discussion as well as experimental results in the next section.

4 Unlocking Data-Centric Generalizable View Synthesis

Motivated by the findings discussed in Section 3, we propose UP-LVSM (Unposed Large View Synthesis Model), a powerful data-centric generalizable NVS framework for the most challenging unposed setting. It eliminates the reliance on 3D knowledge, requiring neither 3D inductive biases nor pose annotations. Unlike the posed-target setting, where supervision on the target pose \mathcal{P} is available, the unposed setting requires to predict a pose $\hat{\mathcal{P}}_{\mathcal{T}}$ for the target image \mathcal{T} . However, due to the absence of the ground truth $\mathcal{P}_{\mathcal{T}}$ for supervision, the learned pose space for $\hat{\mathcal{P}}_{\mathcal{T}}$ could be excessively free and underconstrained, which complicates training. To address this, we propose a novel unposed learning framework as follows, which effectively learns the spatial relationships from 2D imagery.

4.1 Unposed Learning Framework

As illustrated in Figure 6 (a) (b), we build upon existing works [18, 41], employing Transformer to construct our feed-forward neural networks. First, we encode input views into visual tokens using DINOv2 [27] encoders, and then use Transformer to map these tokens to scene latents. A decoder then takes both the scene latents and the latent Plücker representation of the target views as inputs to generate view synthesis results. Here, the latent Plücker representation comes from the *Latent Plücker Learner*, a novel module that learns to construct a latent Plücker presentation for $\mathcal{P}_{\mathcal{T}}$ modeling. As shown in Figure 6 (c), the latent Plücker space is learned from purely 2D imagery supervision in an autoencoder manner. By imposing a bottleneck architecture to constrain the degrees of freedom for the latent Plücker and enforcing the latent space shared across different scenes, our model effectively learns the spatial relationships between views, even in the absence of ground truth 3D supervision. More details about the latent Plücker and camera control are provided in Section 4.3, with specific network architecture provided in the Appendix C.

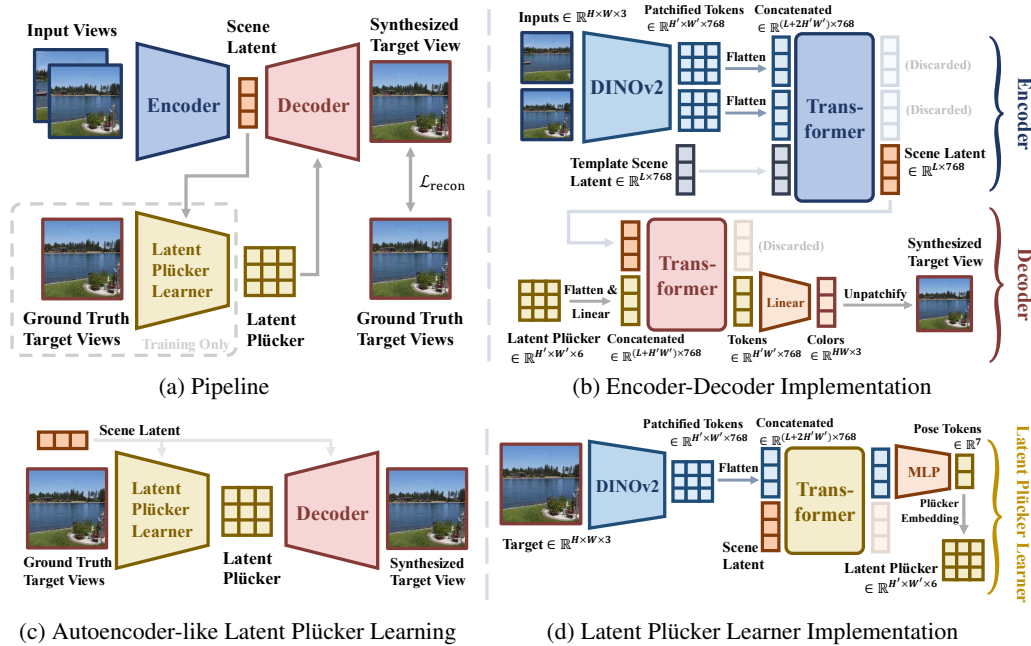


Figure 6: UP-LVSM Overview.

4.2 Experimental Results

Qualitative and quantitative results are shown in Table 3 and Figure 7, respectively. Despite trained without any 3D supervision, our UP-LVSM achieves better performance than posed-target setting methods supervised by ground truth target camera pose. Compared to methods that rely on the input camera poses at inference time, our UP-LVSM even achieves comparable performance without leveraging input poses, while exhibiting promising scalability, following which we can expect the performance gap will be mitigated when available training data scales up in the future. These results demonstrate the effectiveness of our proposed framework, implying the possibility of scaling 2D-only learning frameworks to unlock spatial reasoning without 3D prior knowledge like inductive bias or pose inputs, highlighting a promising direction for future research.

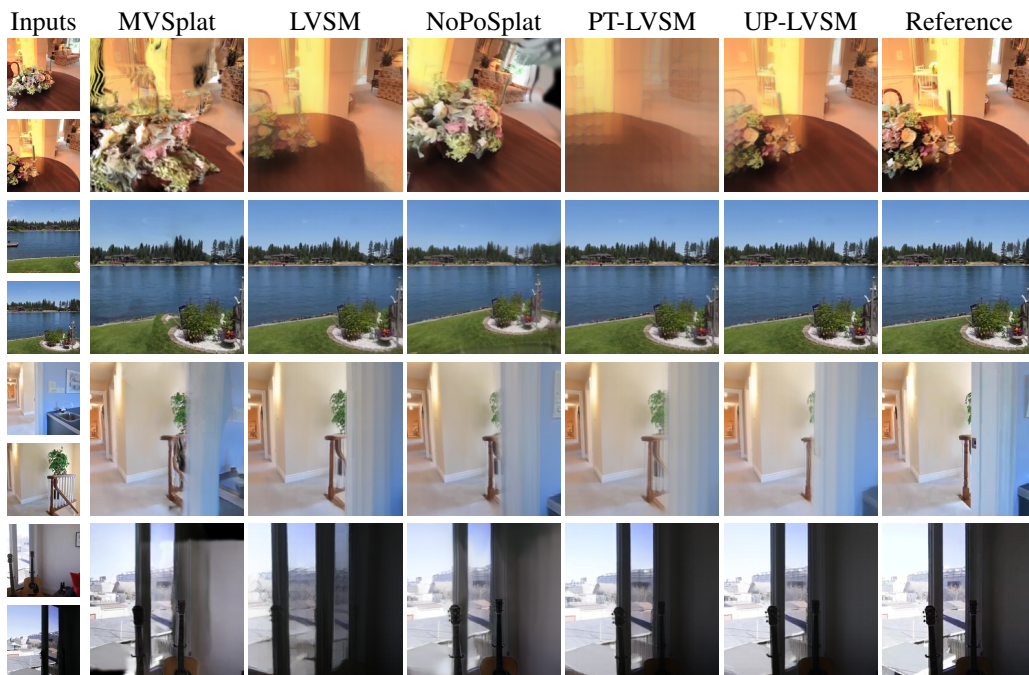


Figure 7: Qualitative View Synthesis Comparisons.

Method	Input Pose	Large Overlap			Medium Overlap			Small Overlap			Full Eval.		
		PSNR \uparrow	SSIM \uparrow	LPIPS \downarrow	PSNR \uparrow	SSIM \uparrow	LPIPS \downarrow	PSNR \uparrow	SSIM \uparrow	LPIPS \downarrow	PSNR \uparrow	SSIM \uparrow	LPIPS \downarrow
PixelNeRF [50]		20.94	0.581	0.517	20.38	0.559	0.540	19.27	0.536	0.568	20.33	0.572	0.549
PixelSplat [5]	✓	26.18	0.879	0.115	23.61	0.821	0.162	21.22	0.752	0.225	25.51	0.867	0.126
MVSplat [6]		27.32	0.889	0.112	23.97	0.819	0.165	20.67	0.730	0.238	26.45	0.874	0.123
LVSM [18]		28.58	0.887	0.108	25.60	0.830	0.149	22.71	0.765	0.202	27.60	0.874	0.117
NoPoSplat [48]		25.84	0.854	0.133	23.67	0.808	0.177	21.58	0.750	0.231	25.46	0.854	0.137
Ours (PT-LVSM)	✗	26.47	0.829	0.130	24.27	0.778	0.173	22.03	0.720	0.224	26.00	0.825	0.135
Ours (UP-LVSM)		29.51	0.901	0.098	26.93	0.852	0.132	24.54	0.796	0.174	28.82	0.891	0.104

Table 3: Quantitative Comparisons on RealEstate10K [55]. Following prior work [48], we conduct evaluations across different overlap levels. Ours achieve comparable performance to posed approaches, particularly in challenging cases where input views share minimal overlap.

4.3 More Investigation & Discussion

Attention Weight Analysis To verify that our method really learn 3D knowledge from 2D training data, we analyze the attention layers of the Transformer network and visualized the attention weights to confirm that the model has a certain understanding of 3D spatial relationships. Specifically, Figure 8 shows the cross-view attention weights, where regions with higher attention correspond to the same area in 3D space. The visualization demonstrates our method learns excellent 3D spatial correspondence, which is essential for camera prediction and novel view synthesis. We further conduct ablation studies by comparing similarity of DINOv2 [27] features (*dinov2_vitb14_reg4_pretrain.pth*) across views to confirm the reliability of our conclusion, validating that UP-LVSM can indeed learn 3D knowledge from 2D training data without 3D supervision. We provide more details in Appendix D.1.



Figure 8: **Attention Visualization.** We visualize the attention weights between the marked patch (red) in the reference view and each patch in the source view. In the colormap, yellow represents high weights, while purple indicates zero. Compared to the feature similarity of DINOv2, our attention map reveal much clearer and more accurate cross-view correspondences. This demonstrates that our proposed method indeed learns 3D knowledge from 2D images without 3D supervision.

Camera-controllable Rendering Earlier work [33] also attempts to learn a latent pose, but typically fails to provide explicit camera control for view synthesis, primarily due to the uninterpretable nature of the learned pose latent. In contrast, our *Latent Plücker Learner* effectively encourage the model to learn a meaningful manifold as latent space, enabling controllability. Specifically, we visualize the learned latent Plücker along with its corresponding ground truth Plücker, as shown in Figure 9 (a), where we sample a set of latent Plücker rays along with their ground-truth counterparts, and apply t-SNE [38] to project the high-dimensional pairs onto a 2D plane with corresponding data points indicated with matching colors. The visualization reveals that the learned latent space aligns with the ground-truth space through a twisted domain transformation, providing further evidence that the model captures the underlying 3D pose space using only 2D supervision. Building on this, we finetune our model with a learnable linear mapper on a small amount of posed data. With this mapper,

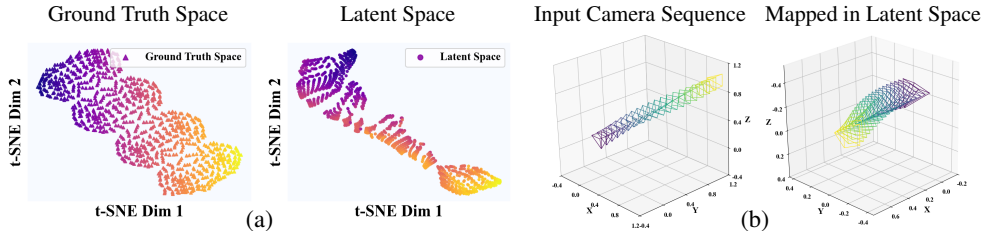


Figure 9: **Camera Control.** (a) The t-SNE [38] visualization shows the learned latent space aligns with the ground-truth space through a twisted domain transformation. (b) A linear mapping can help convert input camera sequence into latent space, facilitating explicit camera control.

we can conduct explicit camera controlling on the real Plücker space and generate the corresponding latent Plücker for the decoder to synthesize novel view, as illustrated in 9 (b). More discussions are provided in Appendix B.

Latent Plücker Details The Plücker ray embedding [28] is a widely used technique to embed camera pose information at the pixel level [53, 18, 41, 25]. Given an image $\mathcal{I} \in \mathbb{R}^{H \times W \times 3}$, the Plücker ray encodes its corresponding pose for each pixel as $\hat{\mathcal{P}} = \text{concat}(\mathbf{o} \times \mathbf{d}, \mathbf{d}) \in \mathbb{R}^{H \times W \times 6}$, where \mathbf{o} represents the camera center and \mathbf{d} is the camera ray direction corresponding to the pixel. Due to the absence of ground truth target pose during training, our *Latent Plücker Learner* first estimates a compact camera vector in the latent space, and then upsample it onto pixel-level Plücker, achieving desirable fine-grained estimation while avoiding excessive degrees of freedom. Consistent with VGGsFM [40], we construct our latent camera vector as $\text{concat}(\mathbf{x}, \mathbf{q}) \in \mathbb{R}^7$, where \mathbf{x} denotes 3D translation and \mathbf{q} is a unit quaternion representing rotation. Figure 9 show that the proposed design learns a geometrically meaningful camera manifold and lays a solid foundation for camera-level controllability. More details are provided in Appendix D.2.

Scalability Discussion Lastly, we compare the scalability of LVSM, PT-LVSM, and UP-LVSM in Figure 10. The results further validate our hypothesis, where a consistent trend is uncovered that methods with the less 3D knowledge dependence exhibit greater scalability. Notably, despite lacking pose information during both training and inference, our UP-LVSM eventually outperforms LVSM at large data scales.

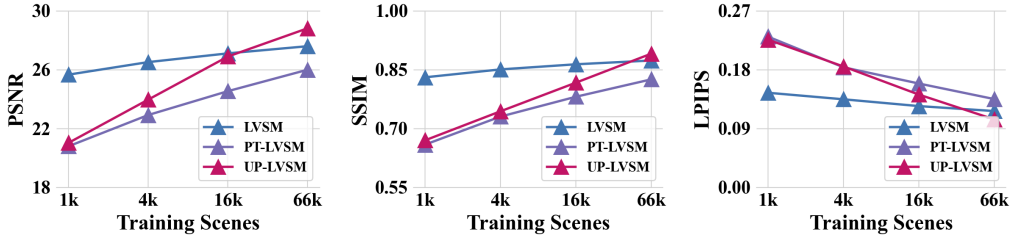


Figure 10: Scalability Comparison of Implicit Methods.

5 Related Work

Generalizable Novel View Synthesis Recent advancements in novel view synthesis using dense multi-view inputs have made significant progress [26, 1, 20, 52], but their reliance on explicit geometric cues limits applicability to unstructured observations. In contrast, generalizable methods aim to bypass computationally expensive per-scene optimization, typically by combining neural networks with 3D representations [50, 42, 13, 5, 6, 46, 53, 48]. Another paradigm [10, 31–33, 36, 18] explores geometry-free solutions using feed-forward neural networks, with the recent method [18] achieving impressive results without explicit 3D bias.

Multi-view Imagery Dataset Learning-based novel view synthesis approaches typically rely on large-scale datasets consisting of multi-view images and their corresponding camera parameters for training. Early datasets focused on object-level data [4, 29, 7, 11], while recent efforts [51, 9] have significantly expanded data scales. Meanwhile, several scene-level datasets [8, 3, 21, 47, 22, 24, 30, 49, 23, 37] have been proposed to facilitate scene-level view synthesis. Among them, the RealEstate10K dataset [55] has garnered significant attention due to its early release, open-source nature, and massive size, becoming a widely used training set and benchmark for recent generalizable view synthesis methods [50, 5, 6, 48, 18].

Pose-free View Synthesis Despite efforts to reduce dependence on input camera poses during inference [14, 35, 48, 54], generalizable novel view synthesis methods typically depend on posed data for training supervision, with few tackling the elimination of pose annotations. Early work [33] pioneered the *really unposed* setting, bypassing pose dependence even during training. However, their solution struggles with high-fidelity rendering, and the latent pose representation remains difficult to interpret, making direct camera pose control challenging. In contrast, our data-centric framework harnesses scalability and the *Latent Plücker Learner* design, achieving rendering quality comparable to methods requiring pose input or supervision [48, 18]. While our design emphasizes camera control, the critical trend uncovered by our investigation is also confirmed by a concurrent work [17] with

their focus on multiple sparse views ($N \geq 5$), achieving promising results at the setting of bypassing 3D supervision.

6 Conclusion

In this work, we revisit the field of generalizable view synthesis through the lens of 3D knowledge. We first highlight the need to reduce dependence on 3D knowledge by analyzing the scaling behaviors of state-of-the-art methods, revealing a key trend: methods with less 3D dependence accelerate dramatically as data scales—*the less you depend, the more you learn*. Building on this, we propose a novel NVS framework that eliminates any 3D inductive bias and camera pose. By eliminating 3D knowledge reliance, our method leverages data scaling to foster implicit 3D awareness from 2D imagery, achieving performance on par with the 3D knowledge-driven counterparts, thereby validating the feasibility and effectiveness of our data-centric paradigm.

Limitation & Future Research In this work, we uncover the key trend that reducing dependence on 3D knowledge improves scalability, but leaving the underlying mechanism underexplored—what exactly drives the scalability advantage of pose-free learning? While collecting large-scale image data with noise-free, scale-consistent poses is impractical, we hypothesize that the scalability of NVS methods may relate to imperfect and inconsistent pose annotations (*e.g.*, those from structure-from-motion methods). Nevertheless, we believe this warrants further investigation and is a promising direction, such as analyzing how pose annotations affect scalability and how these issues might be mitigated by combining our 3D-supervision-free approach with supervised 3D learning, leveraging the benefits of both. More discussions are provided in Appendix F & G.

References

- [1] Jonathan T Barron, Ben Mildenhall, Dor Verbin, Pratul P Srinivasan, and Peter Hedman. Mip-nerf 360: Unbounded anti-aliased neural radiance fields. In *Proceedings of the IEEE/CVF conference on computer vision and pattern recognition*, pages 5470–5479, 2022.
- [2] Eric Brachmann, Jamie Wynn, Shuai Chen, Tommaso Cavallari, Áron Monszpart, Daniyar Turmukhambetov, and Victor Adrian Prisacariu. Scene coordinate reconstruction: Posing of image collections via incremental learning of a relocalizer. In *European Conference on Computer Vision*, pages 421–440. Springer, 2024.
- [3] Angel Chang, Angela Dai, Thomas Funkhouser, Maciej Halber, Matthias Niessner, Manolis Savva, Shuran Song, Andy Zeng, and Yinda Zhang. Matterport3d: Learning from rgb-d data in indoor environments. *arXiv preprint arXiv:1709.06158*, 2017.
- [4] Angel X Chang, Thomas Funkhouser, Leonidas Guibas, Pat Hanrahan, Qixing Huang, Zimo Li, Silvio Savarese, Manolis Savva, Shuran Song, Hao Su, et al. Shapenet: An information-rich 3d model repository. *arXiv preprint arXiv:1512.03012*, 2015.
- [5] David Charatan, Sizhe Li, Andrea Tagliasacchi, and Vincent Sitzmann. pixelsplat: 3d gaussian splats from image pairs for scalable generalizable 3d reconstruction. In *CVPR*, 2024.
- [6] Yuedong Chen, Haofei Xu, Chuanxia Zheng, Bohan Zhuang, Marc Pollefeys, Andreas Geiger, Tat-Jen Cham, and Jianfei Cai. Mvsplat: Efficient 3d gaussian splatting from sparse multi-view images. *arXiv preprint arXiv:2403.14627*, 2024.
- [7] Jasmine Collins, Shubham Goel, Kenan Deng, Achleshwar Luthra, Leon Xu, Erhan Gundogdu, Xi Zhang, Tomas F Yago Vicente, Thomas Dideriksen, Himanshu Arora, et al. Abo: Dataset and benchmarks for real-world 3d object understanding. In *Proceedings of the IEEE/CVF conference on computer vision and pattern recognition*, pages 21126–21136, 2022.
- [8] Angela Dai, Angel X Chang, Manolis Savva, Maciej Halber, Thomas Funkhouser, and Matthias Nießner. Scannet: Richly-annotated 3d reconstructions of indoor scenes. In *Proceedings of the IEEE conference on computer vision and pattern recognition*, pages 5828–5839, 2017.
- [9] Matt Deitke, Ruoshi Liu, Matthew Wallingford, Huong Ngo, Oscar Michel, Aditya Kusupati, Alan Fan, Christian Laforte, Vikram Voleti, Samir Yitzhak Gadre, et al. Objaverse-xl: A universe of 10m+ 3d objects. *Advances in Neural Information Processing Systems*, 36:35799–35813, 2023.
- [10] Alexey Dosovitskiy, Lucas Beyer, Alexander Kolesnikov, Dirk Weissenborn, Xiaohua Zhai, Thomas Unterthiner, Mostafa Dehghani, Matthias Minderer, Georg Heigold, Sylvain Gelly, et al. An image is worth 16x16 words: Transformers for image recognition at scale. *arXiv preprint arXiv:2010.11929*, 2020.

- [11] Laura Downs, Anthony Francis, Nate Koenig, Brandon Kinman, Ryan Hickman, Krista Reymann, Thomas B McHugh, and Vincent Vanhoucke. Google scanned objects: A high-quality dataset of 3d scanned household items. In *2022 International Conference on Robotics and Automation (ICRA)*, pages 2553–2560. IEEE, 2022.
- [12] Yilun Du, Cameron Smith, Ayush Tewari, and Vincent Sitzmann. Learning to render novel views from wide-baseline stereo pairs. In *Proceedings of the IEEE/CVF Conference on Computer Vision and Pattern Recognition*, 2023.
- [13] Yilun Du, Cameron Smith, Ayush Tewari, and Vincent Sitzmann. Learning to render novel views from wide-baseline stereo pairs. In *Proceedings of the IEEE/CVF Conference on Computer Vision and Pattern Recognition*, pages 4970–4980, 2023.
- [14] Zhiwen Fan, Panwang Pan, Peihao Wang, Yifan Jiang, Hanwen Jiang, Dejia Xu, Zehao Zhu, Dilin Wang, and Zhangyang Wang. Pose-free generalizable rendering transformer. *arXiv preprint arXiv:2310.03704*, 2023.
- [15] Zhiwen Fan, Wenyan Cong, Kairun Wen, Kevin Wang, Jian Zhang, Xinghao Ding, Danfei Xu, Boris Ivanovic, Marco Pavone, Georgios Pavlakos, et al. Instantsplat: Unbounded sparse-view pose-free gaussian splatting in 40 seconds. *arXiv preprint arXiv:2403.20309*, 2(3):4, 2024.
- [16] Alex Henry, Prudhvi Raj Dachapally, Shubham Pawar, and Yuxuan Chen. Query-key normalization for transformers. *arXiv preprint arXiv:2010.04245*, 2020.
- [17] Hanwen Jiang, Hao Tan, Peng Wang, Haian Jin, Yue Zhao, Sai Bi, Kai Zhang, Fujun Luan, Kalyan Sunkavalli, Qixing Huang, and Georgios Pavlakos. Rayzer: A self-supervised large view synthesis model, 2025.
- [18] Haian Jin, Hanwen Jiang, Hao Tan, Kai Zhang, Sai Bi, Tianyuan Zhang, Fujun Luan, Noah Snavely, and Zexiang Xu. Lvsm: A large view synthesis model with minimal 3d inductive bias. In *The Thirteenth International Conference on Learning Representations*, 2025.
- [19] Justin Johnson, Alexandre Alahi, and Li Fei-Fei. Perceptual losses for real-time style transfer and super-resolution. In *Computer Vision—ECCV 2016: 14th European Conference, Amsterdam, The Netherlands, October 11–14, 2016, Proceedings, Part II 14*, pages 694–711. Springer, 2016.
- [20] Bernhard Kerbl, Georgios Kopanas, Thomas Leimkühler, and George Drettakis. 3d gaussian splatting for real-time radiance field rendering. *ACM Transactions on Graphics*, 42(4), 2023.
- [21] Zhengqi Li and Noah Snavely. Megadepth: Learning single-view depth prediction from internet photos. In *Proceedings of the IEEE conference on computer vision and pattern recognition*, pages 2041–2050, 2018.
- [22] Zhengqin Li, Ting-Wei Yu, Shen Sang, Sarah Wang, Meng Song, Yuhan Liu, Yu-Ying Yeh, Rui Zhu, Nitesh Gundavarapu, Jia Shi, et al. Openrooms: An open framework for photorealistic indoor scene datasets. In *Proceedings of the IEEE/CVF conference on computer vision and pattern recognition*, pages 7190–7199, 2021.
- [23] Lu Ling, Yichen Sheng, Zhi Tu, Wentian Zhao, Cheng Xin, Kun Wan, Lantao Yu, Qianyu Guo, Zixun Yu, Yawen Lu, et al. DI3dv-10k: A large-scale scene dataset for deep learning-based 3d vision. In *Proceedings of the IEEE/CVF Conference on Computer Vision and Pattern Recognition*, pages 22160–22169, 2024.
- [24] Andrew Liu, Richard Tucker, Varun Jampani, Ameesh Makadia, Noah Snavely, and Angjoo Kanazawa. Infinite nature: Perpetual view generation of natural scenes from a single image. In *Proceedings of the IEEE/CVF International Conference on Computer Vision*, pages 14458–14467, 2021.
- [25] Yuanxun Lu[†], Jingyang Zhang, Tian Fang, Jean–Daniel Nahmias, Yanghai Tsin, Long Quan[‡], Xun Cao[†], Yao Yao[†], and Shiwei Li. Matrix3d: Large photogrammetry model all-in-one. In *CVPR*, 2025.
- [26] Ben Mildenhall, Pratul P. Srinivasan, Matthew Tancik, Jonathan T. Barron, Ravi Ramamoorthi, and Ren Ng. NeRF: Representing scenes as neural radiance fields for view synthesis. In *The European Conference on Computer Vision (ECCV)*, 2020.
- [27] Maxime Oquab, Timothée Darcet, Théo Moutakanni, Huy Vo, Marc Szafraniec, Vasil Khalidov, Pierre Fernandez, Daniel Haziza, Francisco Massa, Alaaeldin El-Nouby, et al. Dinov2: Learning robust visual features without supervision. *arXiv preprint arXiv:2304.07193*, 2023.
- [28] Julius Plucker. Xvii. on a new geometry of space. *Philosophical Transactions of the Royal Society of London*, 155:725–791, 1865.

- [29] Jeremy Reizenstein, Roman Shapovalov, Philipp Henzler, Luca Sbordone, Patrick Labatut, and David Novotny. Common objects in 3d: Large-scale learning and evaluation of real-life 3d category reconstruction. In *Proceedings of the IEEE/CVF international conference on computer vision*, pages 10901–10911, 2021.
- [30] Mike Roberts, Jason Ramapuram, Anurag Ranjan, Atulit Kumar, Miguel Angel Bautista, Nathan Paczan, Russ Webb, and Joshua M Susskind. Hypersim: A photorealistic synthetic dataset for holistic indoor scene understanding. In *Proceedings of the IEEE/CVF international conference on computer vision*, pages 10912–10922, 2021.
- [31] Robin Rombach, Patrick Esser, and Björn Ommer. Geometry-free view synthesis: Transformers and no 3d priors. In *Proceedings of the IEEE/CVF International Conference on Computer Vision*, pages 14356–14366, 2021.
- [32] Mehdi S. M. Sajjadi, Henning Meyer, Etienne Pot, Urs Bergmann, Klaus Greff, Noha Radwan, Suhani Vora, Mario Lucic, Daniel Duckworth, Alexey Dosovitskiy, Jakob Uszkoreit, Thomas Funkhouser, and Andrea Tagliasacchi. Scene Representation Transformer: Geometry-Free Novel View Synthesis Through Set-Latent Scene Representations. *CVPR*, 2022.
- [33] Mehdi S. M. Sajjadi, Aravindh Mahendran, Thomas Kipf, Etienne Pot, Daniel Duckworth, Mario Lučić, and Klaus Greff. RUST: Latent Neural Scene Representations from Unposed Imagery. *CVPR*, 2023.
- [34] Johannes L Schonberger and Jan-Michael Frahm. Structure-from-motion revisited. In *Proceedings of the IEEE conference on computer vision and pattern recognition*, pages 4104–4113, 2016.
- [35] Brandon Smart, Chuanxia Zheng, Iro Laina, and Victor Adrian Prisacariu. Splatt3r: Zero-shot gaussian splatting from uncalibrated image pairs. *arXiv preprint arXiv:2408.13912*, 2024.
- [36] Mohammed Suhail, Carlos Esteves, Leonid Sigal, and Ameesh Makadia. Generalizable patch-based neural rendering. In *European Conference on Computer Vision*, pages 156–174. Springer, 2022.
- [37] Joseph Tung, Gene Chou, Ruojin Cai, Guandao Yang, Kai Zhang, Gordon Wetzstein, Bharath Hariharan, and Noah Snavely. Megascenes: Scene-level view synthesis at scale. In *ECCV*, 2024.
- [38] Laurens Van der Maaten and Geoffrey Hinton. Visualizing data using t-sne. *Journal of machine learning research*, 9(11), 2008.
- [39] Ashish Vaswani, Noam Shazeer, Niki Parmar, Jakob Uszkoreit, Llion Jones, Aidan N Gomez, Łukasz Kaiser, and Illia Polosukhin. Attention is all you need. *Advances in neural information processing systems*, 30, 2017.
- [40] Jianyuan Wang, Nikita Karaev, Christian Rupprecht, and David Novotny. Vggsfm: Visual geometry grounded deep structure from motion. In *Proceedings of the IEEE/CVF Conference on Computer Vision and Pattern Recognition*, pages 21686–21697, 2024.
- [41] Jianyuan Wang, Minghao Chen, Nikita Karaev, Andrea Vedaldi, Christian Rupprecht, and David Novotny. Vggt: Visual geometry grounded transformer. In *Proceedings of the IEEE/CVF Conference on Computer Vision and Pattern Recognition*, 2025.
- [42] Qianqian Wang, Zhicheng Wang, Kyle Genova, Pratul P Srinivasan, Howard Zhou, Jonathan T Barron, Ricardo Martin-Brualla, Noah Snavely, and Thomas Funkhouser. Ibrnet: Learning multi-view image-based rendering. In *Proceedings of the IEEE/CVF conference on computer vision and pattern recognition*, pages 4690–4699, 2021.
- [43] Shuzhe Wang, Vincent Leroy, Yohann Cabon, Boris Chidlovskii, and Jerome Revaud. Dust3r: Geometric 3d vision made easy. In *CVPR*, 2024.
- [44] Zirui Wang, Shangzhe Wu, Weidi Xie, Min Chen, and Victor Adrian Prisacariu. NeRF—: Neural radiance fields without known camera parameters. *arXiv preprint arXiv:2102.07064*, 2021.
- [45] Christopher Wewer, Kevin Raj, Eddy Ilg, Bernt Schiele, and Jan Eric Lenssen. latentsplat: Autoencoding variational gaussians for fast generalizable 3d reconstruction. In *European Conference on Computer Vision*, pages 456–473. Springer, 2024.
- [46] Haofei Xu, Anpei Chen, Yuedong Chen, Christos Sakaridis, Yulun Zhang, Marc Pollefeys, Andreas Geiger, and Fisher Yu. Murf: multi-baseline radiance fields. In *Proceedings of the IEEE/CVF Conference on Computer Vision and Pattern Recognition*, pages 20041–20050, 2024.
- [47] Yao Yao, Zixin Luo, Shiwei Li, Jingyang Zhang, Yufan Ren, Lei Zhou, Tian Fang, and Long Quan. Blendedmvs: A large-scale dataset for generalized multi-view stereo networks. In *Proceedings of the IEEE/CVF conference on computer vision and pattern recognition*, pages 1790–1799, 2020.

- [48] Botao Ye, Sifei Liu, Haofei Xu, Xueting Li, Marc Pollefeys, Ming-Hsuan Yang, and Songyou Peng. No pose, no problem: Surprisingly simple 3d gaussian splats from sparse unposed images. In *The Thirteenth International Conference on Learning Representations*, 2025.
- [49] Chandan Yeshwanth, Yueh-Cheng Liu, Matthias Nießner, and Angela Dai. Scannet++: A high-fidelity dataset of 3d indoor scenes. In *Proceedings of the IEEE/CVF International Conference on Computer Vision*, pages 12–22, 2023.
- [50] Alex Yu, Vickie Ye, Matthew Tancik, and Angjoo Kanazawa. pixelNeRF: Neural radiance fields from one or few images. In *CVPR*, 2021.
- [51] Xianggang Yu, Mutian Xu, Yidan Zhang, Haolin Liu, Chongjie Ye, Yushuang Wu, Zizheng Yan, Chenming Zhu, Zhangyang Xiong, Tianyou Liang, et al. Mvimagnet: A large-scale dataset of multi-view images. In *Proceedings of the IEEE/CVF conference on computer vision and pattern recognition*, pages 9150–9161, 2023.
- [52] Zehao Yu, Anpei Chen, Binbin Huang, Torsten Sattler, and Andreas Geiger. Mip-splatting: Alias-free 3d gaussian splatting. In *Proceedings of the IEEE/CVF conference on computer vision and pattern recognition*, pages 19447–19456, 2024.
- [53] Kai Zhang, Sai Bi, Hao Tan, Yuanbo Xiangli, Nanxuan Zhao, Kalyan Sunkavalli, and Zexiang Xu. Gs-lrm: Large reconstruction model for 3d gaussian splatting. *European Conference on Computer Vision*, 2024.
- [54] Shangzhan Zhang, Jianyuan Wang, Yinghao Xu, Nan Xue, Christian Rupprecht, Xiaowei Zhou, Yujun Shen, and Gordon Wetzstein. Flare: Feed-forward geometry, appearance and camera estimation from uncalibrated sparse views. *arXiv preprint arXiv:2502.12138*, 2025.
- [55] Tinghui Zhou, Richard Tucker, John Flynn, Graham Fyffe, and Noah Snavely. Stereo magnification: learning view synthesis using multiplane images. *ACM Trans. Graph.*, 37(4), 2018.

A Problem Setting Details

In this section, we provide additional details regarding the problem settings described in Section 3 of the main paper, where we present our analysis to support the hypothesis: *The less you depend, the more you learn*. Clarifying these settings is essential, as our analysis relies heavily on experimental results and comparative evaluations across state-of-the-art methods. While Figure 1 in the main paper illustrates the three problem settings we categorize, and Table 1 lists the corresponding methods, the definitions of these settings—such as their inputs, outputs, and evaluation protocols—are only briefly discussed for clarity. In this appendix, we elaborate on these aspects, with particular attention to distinctions between training, evaluation, and real-world deployment.

A.1 Posed Setting

The *posed* setting is the most straightforward scenario, assuming that pose information is always available. During both training and evaluation, the pose of the target view $\mathcal{P}_{\mathcal{T}}$ is provided by the dataset. In real-world applications, however, $\mathcal{P}_{\mathcal{T}}$ is determined by a user query, reflecting natural camera control behavior.

A critical aspect of this setting is that the view synthesis problem is inherently *pose-equivalent*: any given instance with poses $\mathcal{P}_{\mathcal{I}}, \mathcal{P}_{\mathcal{T}}$ is functionally equivalent to one with poses $\mathcal{H}'\mathcal{P}_{\mathcal{I}}, \mathcal{H}'\mathcal{P}_{\mathcal{T}}$, where \mathcal{H}' is an arbitrary transformation in $\text{SE}(3)$. To ensure pose-equivalence during training, a common practice is to apply **camera pose normalization**. This procedure treats the first input view as the reference, designating its pose as canonical and transforming all other camera poses from world coordinates into the canonical frame.

A.2 Posed-Target Setting

The *posed-target* setting introduces a subtle but important distinction. Unlike the posed setting, it does not require the input view poses $\mathcal{P}_{\mathcal{I}}$ for scene modeling, but it does require the target pose $\mathcal{P}_{\mathcal{T}}$ for view synthesis. Despite the pose-equivalence normalization discussed earlier, this setting inherently introduces ambiguity—specifically, how can a model reason about the spatial relationship between a posed target view and unposed input views?

To address this challenge, existing posed-target methods [44, 15, 48] typically employ an **evaluation-time pose alignment** trick to ensure fair comparison on benchmarks such as RealEstate10K [55]. For example, in NoPoSplat [48], the model first estimates a 3D Gaussian Splatting (3DGS) representation in a canonical space from two unposed input views. This reconstructed 3DGS is then frozen, and the target camera pose is optimized at inference time so that the synthesized target view aligns as closely as possible with the ground truth image. It is important to note that this procedure is used solely for benchmark evaluation; in real-world applications, the target view pose is typically determined directly via user input, making such optimization unnecessary.

A.3 Unposed Setting

The *unposed* setting presents the most challenging scenario. Unlike the posed-target setting, where the target view pose $\mathcal{P}_{\mathcal{T}}$ is known and can guide view synthesis, the unposed setting assumes no pose information is available even during training, leaving explicit pose-based viewpoint control impossible.

To overcome this limitation, the early method, RUST [33], employs a strategy similar to evaluation-time alignment, but adapted for training. Specifically, RUST introduces an implicit alignment mechanism by allowing the model to observe the ground truth target image $\tilde{\mathcal{T}}$ and learn to estimate its pose in a self-supervised manner, as depicted in Figure 1 of the main paper. Following this, our UP-LVSM framework introduces the *Latent Plücker Learner*, which estimates latent Plücker coordinates from the target view $\tilde{\mathcal{T}}$ and the scene latent \mathcal{S} . This design enables the model to infer the viewpoint from which to render, facilitating implicit alignment between the synthesized and ground truth target views for effective supervision. The concurrent work, Rayzer [17], adopts a similar strategy by inferring the spatial relationship from multiple input and target views to predict each view’s corresponding Plücker maps for view synthesis.

While such alignment techniques are effective during training and evaluation, they are unsuitable for real-world deployment, where the ground truth target view is unavailable. Unlike the posed and

posed-target settings, where the target pose can be explicitly determined via human-specified camera sequences, the unposed setting relies on a learned, implicit pose space. This fundamentally limits direct, interpretable control and thereby weakens its practical applicability. To address this, our work prioritizes explicit camera control over implicit solutions [33] or relative ones [17], and proposes an effective strategy, which we detail in Appendix B.

B Camera Control Details

In this section, we describe the extension of UP-LVSM to support camera-controllable rendering in real-world scenarios. As noted in Appendix A.3, the ground-truth target view is unavailable in such settings, precluding the use of the Latent Plücker Learner for target pose alignment. To overcome this limitation, we fine-tune the model with a pose mapper that projects real-world input camera poses into the learned latent space, thereby enabling explicit camera control, as outlined in Section 4.3 of the main paper. Regarding camera intrinsics, we follow NoPoSplat [48] in assuming a known set of intrinsics for simplicity, while it is also feasible to extend the Latent Plücker Learner to accommodate learnable intrinsic.

Specifically, we introduce a linear pose mapper parameterized by $(\mathbf{A} \in \mathbb{R}^{7 \times 7}, \mathbf{b} \in \mathbb{R}^7)$, which maps a real-world camera pose vector $\hat{\mathbf{C}} = \text{concat}(\hat{\mathbf{x}}, \hat{\mathbf{q}}) \in \mathbb{R}^7$ into its corresponding latent representation $\mathbf{C} = \text{concat}(\mathbf{x}, \mathbf{q}) = \mathbf{A}\hat{\mathbf{C}} + \mathbf{b} \in \mathbb{R}^7$. This latent camera pose is then used to generate the associated Plücker representation $\hat{\mathcal{P}}$. We fine-tune UP-LVSM with this linear mapper using a small subset of posed data (1202 scenes in RealEstate10K [55], 1.8% of the training dataset). As described in Appendix A.1, we also apply camera pose normalization to reduce pose ambiguity. Further training details are provided in Appendix C.1.

After fine-tuning, human-specified camera sequences can be directly mapped to latent Plücker representations for view synthesis, as illustrated in Figure 9 (b) of the main paper. This fine-tuning introduces negligible impact on rendering quality (quantitatively $< 1\%$, also as evidenced in Figure 11).

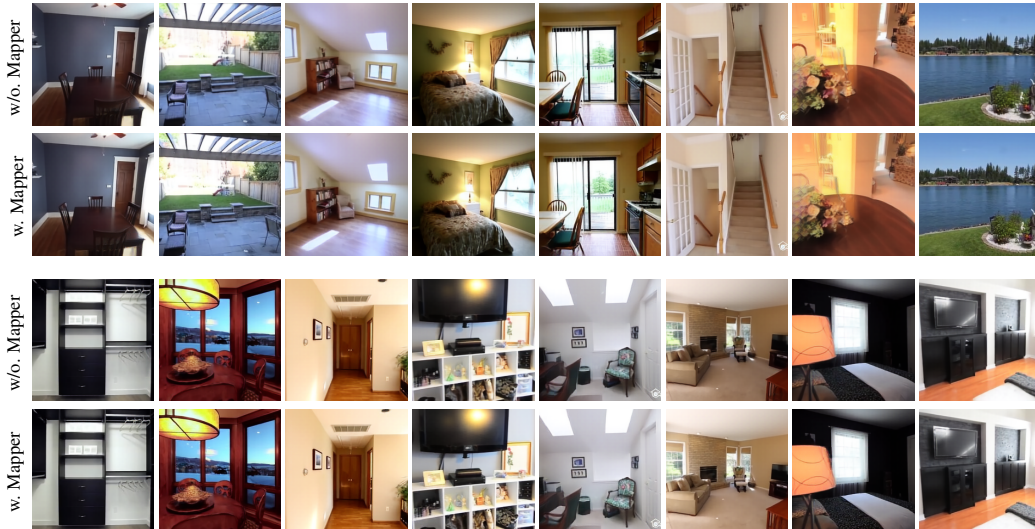


Figure 11: **Ablation Study of Camera Mapper.** The camera mapper fine-tuning introduces negligible impact on rendering quality.

Compared to the earlier unposed method RUST [33], our approach introduces an explicit camera control strategy. In contrast, RUST relies on implicit alignment and is unable to produce accurate renderings without access to the ground truth target view, thereby limiting its applicability in real-world settings. The concurrent work, Rayzer [17], also addresses camera control, but in a relative manner: it first estimates the camera poses of input views and then allows user-specified interpolation between these poses. While effective, this strategy offers less flexibility than

our approach. Additionally, it relies on multiple input views ($N \geq 5$) to infer spatial relationship, while our method only requires two views ($N = 2$).

C Implementation Details

In this section, we provide implementation details for the methods compared in the main paper, including network architectures and training hyperparameters.

C.1 PT-LVSM & UP-LVSM

Following prior works [32, 53, 18], the core architecture of PT-LVSM is composed entirely of Transformer layers [39]. Unlike previous implementations that train the encoder from scratch, we incorporate a pretrained DINOv2 encoder [27] to enhance training stability, particularly in the early stages, due to the absence of input pose annotations. The Transformer component adopts a decoder-only architecture, as in LVSM [18], comprising 24 layers. Each multi-head attention layer includes 12 heads, each with 64-dimensional feature embeddings. The entire model, including both the Transformers and the DINOv2 encoder, is jointly optimized with a learning rate of 0.0004.

Training is conducted on the full RealEstate10K dataset [55] using 8 NVIDIA A100 GPUs, with a batch size of 16 per GPU. Training for 100K steps takes approximately 60 hours. The loss function used is $\mathcal{L} = \text{MSE}(\mathcal{T}, \tilde{\mathcal{T}}) + \lambda \text{Perceptual}(\mathcal{T}, \tilde{\mathcal{T}})$, where $\lambda = 0.5$, and Perceptual denotes the perceptual loss introduced in [19]. For numerical stability, we follow LVSM [18] in employing QKNorm [16] to mitigate the risk of gradient explosion.

The architecture of UP-LVSM differs slightly due to its encoder-decoder structure and latent Plücker representation. The encoder comprises a DINOv2 backbone followed by 6 Transformer layers. The decoder consists of 14 Transformer layers. Additionally, the Latent Plücker Learner uses a DINOv2 encoder followed by a 4-layer Transformer. Note that our number of layers is set equal to LVSM and PT-LVSM for fair comparisons under the same level of parameter amount. All other training settings are consistent with those of PT-LVSM. After pretraining, UP-LVSM is fine-tuned to support camera-controllable rendering using a linear mapper. This fine-tuning is performed on the *little* subset of the RealEstate10K dataset (1202 scenes, 1.8% of the full set) with a learning rate of 0.0001, requiring approximately 4 hours for 8K steps. During this stage, the ground truth target image is no longer provided; instead, the latent Plücker is generated via the linear mapper from the ground truth target pose, rather than from the Latent Plücker Learner.

For both PT-LVSM and UP-LVSM, we adopt camera pose normalization mentioned in Appendix A.1 to designate the pose of the first input view as canonical. However, this conflicts with the permutation-invariant nature of the Transformer, where the first input view should be recognized as special, but the Transformer inherently treats all inputs equally. To this end, we assign special significance to the first view by adding a linearly projected canonical Plücker onto its DINOv2 image tokens. The ablation study demonstrates our model cannot converge when trained without this trick, validating its effectiveness.

Lastly, due to the DINOv2 encoder’s requirement that input dimensions be divisible by the patch size of 14, we rescale RealEstate10K images to a resolution of 224×224 , rather than the more commonly used 256×256 . Following the approach in LVSM, we first train at low resolution (e.g., 224×224), and then fine-tune on higher resolutions such as 518×518 to better adapt the model to high-resolution rendering. However, for the experiments reported in the main paper, we standardize all evaluations to the 224×224 setting, including all baseline comparisons.

C.2 Baselines

For all baseline methods evaluated in the main paper—PixelNeRF [50], PixelSplat [5], MVSplat [6], LVSM [18], and NoPoSplat [48]—we use the original training configurations provided in their respective official repositories. Since PixelNeRF does not provide official configurations for the RealEstate10K dataset, we adapt its official code to work with this dataset and successfully reproduce the performance reported in [48, 5]. All other methods include official support for the RealEstate10K dataset, requiring no modification aside from rescaling the input images to 224×224 (consistent with our setup as described above).

D Investigation Details

This section provides additional details for the analysis presented in Section 4.3 of the main paper, including attention weight analysis and latent Plücker space analysis.

D.1 Attention Weight Analysis

We elaborate on Figure 8 of the main paper by visualizing patch-wise attention weights to illustrate that our model performs spatial reasoning and captures cross-view correspondences. Below, we describe the process in detail.

Consider an input image resolution of 224. Following the DINOv2 architecture, which uses a patch size of 14, each input image $\mathcal{I} \in \mathbb{R}^{B \times N \times 224 \times 224 \times 3}$ is converted into feature tokens $\mathbf{D} \in \mathbb{R}^{B \times N \times 16 \times 16 \times 768}$, where B is the batch size and N is the number of input views. These tokens are then flattened to $\mathbf{D}' \in \mathbb{R}^{B \times 256 \times N \times 768}$ and passed through the Transformer layers in the encoder.

We examine the attention weights $\mathbf{W} \in \mathbb{R}^{B \times 256 \times N \times 256 \times N}$ from the final Transformer layer, where each element represents the attention between pairs of input patches across all views. In the case where $N = 2$ and $B = 1$, the bottom-left 256×256 block of \mathbf{W} , denoted as $\mathbf{W}' \in \mathbb{R}^{256 \times 256}$, corresponds to the cross-view attention between the two input views. Specifically, each element $\mathbf{W}(i, j)$ indicates the attention weight from the i -th patch of the first view to the j -th patch of the second view.

While we use the *viridis* colormap to visualize the attention weights \mathbf{W} in Figure 8 of the main paper, we also visualize the DINOv2 token similarity to verify that the model learns cross-view correspondence during training, rather than relying solely on the pretrained DINOv2 encoder’s inherent capabilities. Specifically, given DINOv2 tokens $\mathbf{D}'_1, \mathbf{D}'_2 \in \mathbb{R}^{256 \times 768}$ from two views, we compute their cosine similarity along the feature dimension to obtain $\mathbf{S} \in \mathbb{R}^{256 \times 256}$. For clearer visualization, \mathbf{S} is normalized as $\mathbf{S}' = \frac{\mathbf{S} - \min(\mathbf{S})}{\max(\mathbf{S}) - \min(\mathbf{S})}$.

D.2 Latent Plücker Analysis

Here, we elaborate on Figure 9 (a) from the main paper. Camera poses are represented as 7-dimensional vectors, with the first 3 dimensions encoding translation and the last 4 representing rotation as a quaternion. Given N pairs of camera poses $\mathbf{C}_{\text{latent}} \in \mathbb{R}^{N \times 7}$ and $\mathbf{C}_{\text{real}} \in \mathbb{R}^{N \times 7}$, we concatenate them to form $\mathbf{C}_{\text{all}} \in \mathbb{R}^{2N \times 7}$. We then apply t-SNE [38] to project this 7-dimensional space into two dimensions, yielding $\mathbf{C}'_{\text{latent}}, \mathbf{C}'_{\text{real}} \in \mathbb{R}^{N \times 2}$ after splitting. In Figure 9 (a), these 2D points are visualized accordingly, with corresponding pairs colored identically.

E More Discussion about Extrapolation

All the view synthesis results in the main paper or the supplementary video are mainly interpolation between inputs views. This is because currently, most existing generalizable novel view synthesis (NVS) methods are good at interpolation-style NVS, but perform much worse for extrapolation, as extrapolation is actually guessing what the whole scenes look like from partial observation, thereby indeed requiring generative modeling techniques [45]. Our methods suffer from the similar problem. Following extrapolation evaluation principles in previous work [45], we measure the extrapolation performance of existing methods. Table 4 compares the interpolation and extrapolation performance, demonstrating fundamental limitations of these generalizable methods.

Evaluation	Metric	PixelNeRF [50]	PixelSplat [5]	MVSplat [6]	LVSM [18]	NoPoSplat [48]	Ours (PT-LVSM)	Ours (UP-LVSM)
Interpolation	PSNR \uparrow	20.33	25.51	26.45	27.60	25.46	26.00	28.82
	SSIM \uparrow	0.572	0.867	0.874	0.874	0.854	0.825	0.891
	LPIPS \downarrow	0.549	0.126	0.123	0.117	0.137	0.135	0.104
Extrapolation	PSNR \uparrow	19.96	21.19	20.00	23.80	22.42	19.18	23.82
	SSIM \uparrow	0.572	0.799	0.787	0.795	0.786	0.611	0.760
	LPIPS \downarrow	0.568	0.196	0.205	0.168	0.201	0.282	0.185

Table 4: **Quantitative Comparisons.** Existing methods perform much worse for extrapolation.

F More Discussion about Scalability

In this section, we further explore the scalability analysis presented in Section 3 of the main paper. A key observation from Figure 3 is that data-centric methods, such as LVSM and PT-LVSM, demonstrate more significant acceleration compared to bias-driven methods, such as MVSPlat and NoPoSplat, as the dataset size increases. Currently, it is challenging to extend these scalability comparisons to larger datasets, primarily due to the limited availability of open-source datasets containing real-world imagery data at scales exceeding that of RealEstate10K. However, we anticipate that the availability of such data will expand significantly in the future, enabling more comprehensive analyses, including the scaling behavior of various network parameters. In this paper, we refrain from varying the network capacity for each method, as we argue that it is a fair comparison to use the maximum network capacity originally designed for the RealEstate10K dataset across all baselines.

Although we cannot yet validate this trend at larger scales, we observe a promising pattern: posed-setting methods tend to exhibit poorer scalability. We attribute this to the quality of training data, particularly the incorrect pose annotations often produced by Structure-from-Motion (SfM) preprocessing tools, such as COLMAP [34]. Posed-setting methods are more susceptible to performance degradation due to such inaccuracies. To validate this hypothesis, we investigate the impact of pose noise on LVSM performance, with experimental results presented in Figure 12. These results show that even a small amount of noise significantly affects LVSM’s performance. This provides partial insight into the trend observed in Figure 5 of the main paper, where methods that do not rely on input poses (e.g., PT-LVSM) eventually outperform those that depend on poses, even when the latter have access to additional information.

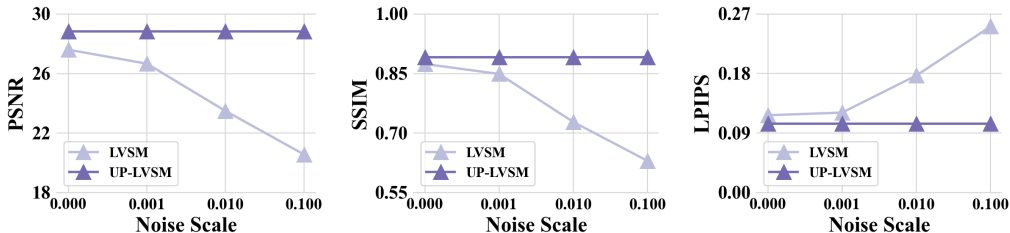


Figure 12: **Performance of Methods Trained with Noisy Poses.** Different levels of Gaussian noise ($\sigma^2 = 0.001, 0.01, 0.1$) were added to the rotation (in quaternion form) and translation components of the poses in training data. While UP-LVSM remains agnostic to noisy poses, LVSM experiences significant degradation with increasing noise levels, exhibiting sensitivity even to small amounts of noise (0.001).

G More Discussion about Limitation

Lastly, we comprehensively discuss the limitations of our work and potential directions for future research. As mentioned in Section 6 of the main paper, while we identify the key trend that reducing dependence on 3D knowledge enhances scalability, we leave the underlying mechanisms underexplored, offering only hypotheses related to noisy pose annotations (as shown in Figure 12 in Appendix F). Additionally, due to data limitations, we have not yet validated this trend at larger scales, as discussed in Appendix F.

From a methodological standpoint, our UP-LVSM is still based on DINOv2 and inherits its limitation of a relatively large patch size of 14 (compared to LVSM’s patch size of 8). The large patch size hinders fine-granularity image synthesis, leading to blurring artifacts in richly textured areas. As demonstrated in LVSM [18], smaller patch sizes lead to more competitive performance at the cost of increased training time and higher CUDA memory usage. Striking a balance between performance and training cost, particularly through improvements to the network architecture, is an important avenue for future exploration. Furthermore, we observe that increasing the amount of training data increases the risk of gradient explosion. While we mitigate this issue by adopting QKNorm [16] as in LVSM, addressing this issue more effectively, particularly when scaling to larger datasets, will be crucial in future work.